

## INDUSTRIAL N-TYPE PERL CELLS WITH SCREEN PRINTED FRONT SIDE ELECTRODES APPROACHING 21% EFFICIENCY

U. Jäger<sup>1\*</sup>, B. Steinhauser<sup>1</sup>, J. Benick<sup>1</sup>, E. Chong<sup>2</sup>, J. Lam<sup>2</sup>, R. Steeman<sup>2,3</sup>, H. Rostan<sup>2</sup>, J. Nekarda<sup>1</sup>, and M. Hermle<sup>1</sup>

<sup>1</sup>Fraunhofer Institute for Solar Energy Systems ISE, Heidenhofstraße 2, 79110 Freiburg, Germany

<sup>2</sup>REC Solar Pte. Ltd., 20 Tuas South Avenue 14, Singapore 637312, Singapore

<sup>3</sup>Formerly REC Solar Pte. Ltd., now with 1366Technologies, 6 Preston Ct, Bedford, MA 01730, USA

\*Phone: +49 (0)761 4588 5057, e-mail: Ulrich.jaeger@ise.fraunhofer.de

**ABSTRACT:** We discuss the enhancements of firing stable *fPassDop* technology for *n*-type passivated emitter and rear locally diffused (PERL) silicon solar cells. We investigate modifications of the SiN<sub>x</sub> based layer by adjusting the nitrogen content. By modifying the passivation layer stack, we achieve higher doping concentrations after laser doping, which is beneficial for rear electrode contact formation. We also show that we find less nitrogen in the point contacts after laser processing when using the updated layer system. Solar cells results confirm these findings: those using the adapted passivation layer, yield lower ohmic losses as well as less scattering in the fill factor. Cell efficiencies of 20.9% and open circuit voltages of 672 mV are achieved.

**Keywords:** *n*-type, laser processing, passivation

### 1 INTRODUCTION

In recent years, *n*-type silicon has attracted researchers' attention. It offers advantages compared to *p*-type silicon: it is less sensitive to most metal impurities [1] and it does not show significant light induced degradation due to the boron oxygen complex [2, 3]. This allows for high minority carrier diffusion lengths in the bulk making this material highly suitable for advanced high efficiency cell concepts such as interdigitated back contact cells [4] and passivated emitter and rear cell/locally diffused (PERC/PERL) type cells [5-7] as well as bifacial passivated emitter and rear totally diffused (PERT) type cells [8]. However, for the fabrication of a local back surface field (LBSF) in *n*-PERL type cells, thermal phosphorous diffusion with some elaborate structuring technology is generally required.

The *PassDop* sequence allows the lean fabrication of an LBSF for monofacial *n*-type silicon cells with PERL (passivated emitter and rear locally diffused) architecture, as depicted and described in Figure 1. It was introduced by Suwito *et al.* based on phosphorous doped amorphous silicon carbide [9, 10]. Steinhauser *et al.* transferred this to a silicon nitride (SiN<sub>x</sub>) based scheme, proving that a suitable SiN<sub>x</sub> layer stack can withstand a contact firing step without significant loss in passivation quality [11]. These firing stable layers are referred to as "*fPassDop*" layers.

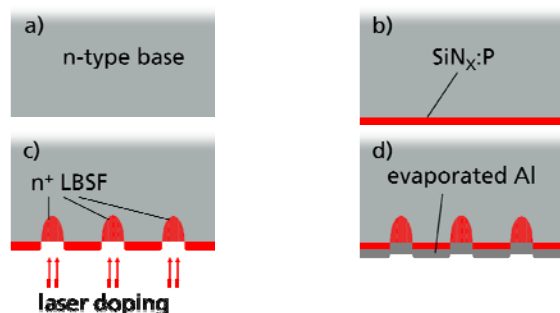


**Figure 1:** The *n*-*PassDop* approach: onto the base of an *n*-type silicon solar cell (a) a phosphorous doped

passivation layer is deposited by PECVD (b), a laser process creates point contacts and dopes the underlying silicon simultaneously (c). Subsequently, a layer of aluminium is evaporated onto the rear side of the device forming the *n*-electrode (d).

In this work, we show the feasibility of fabricating high efficiency *n*-type solar devices featuring PERL cell architecture on large area FZ- and Cz-Si using screen printed front side electrodes.

### 2 INVESTIGATION OF LASER DOPING FROM *PASSDOP* LAYERS

#### 2.1 Firing stable SiN<sub>x</sub> *PassDop* layers

Steinhauser *et al.* already pointed out that it was beneficial to use a stack system to further improve the passivation quality as well as the doping capability of the *PassDop* layer system, going from a single layer system to a two layer system ("Gen1" and further improved to "Gen2") [11].

This layer system ("*fPassDop* Gen2") is deposited by means of plasma enhanced chemical vapor deposition (PECVD). However, this layer stack still yielded low surface dopant concentrations in the LBSF after laser processing therefore enabling only metal-semiconductor contacts of moderate reliability, i.e. partially high specific contact resistivity. This led to a comparably large distribution in fill factor of the solar cells and thus a process of limited stability. Thus, we modified the layer stack ("*fPassDop* Gen3", layers with higher index of refraction compared to Gen2). To investigate the impact of these changes, we prepared samples where we were able to measure the sheet resistance  $R_{\text{sheet}}$  as well the doping profile by both electro-chemical capacitance voltage (ECV) and secondary ion mass spectroscopy (SIMS). We also prepared samples with single point contacts to allow for some energy dispersive x-ray spectroscopy (EDX) to investigate the material composition of the laser doped area. The process flow for these samples is shown in Figure 2. After damage etching in KOH, Cz-Si samples were coated with *fPassDop* layers of Gen2 and Gen3 by means of PECVD. Then,

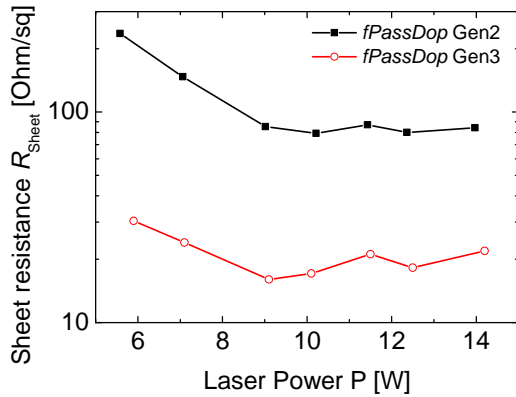
laser processing was carried out using a Jenoptik JenLas IR70 laser ( $\lambda = 1030$  nm,  $f = 30$  kHz) to form fully laser processed areas on the  $p$ -type substrates. These samples were used for characterization of  $R_{\text{sheet}}$  by four point probing (4pp) and profile measurements by ECV and SIMS). On the  $n$ -type substrates, we formed point contacts, allowing a microstructure analysis by scanning electron microscope (SEM) and EDX.

p-type Cz-Si	n-type Cz-Si
KOH damage etch	
PECVD: $fPassDop$ layer deposition	
Laser processing: $2 \times 2$ cm <sup>2</sup>	Laser processing: points
4pp, ECV, SIMS	SEM, EDX

**Figure 2:** Process flow for the samples allowing characterization by 4pp, ECV, SIMS and EDX.

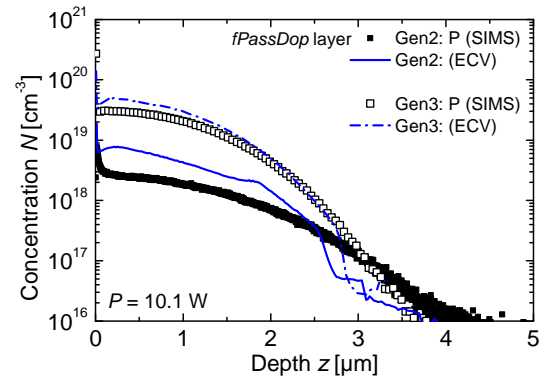
### 2.2 Sheet resistance and electron concentrations

Figure 3 shows the resulting sheet resistance after laser processing of  $fPassDop$  layers Gen2 and Gen3. We observe substantially lower sheet resistances when laser doping from  $fPassDop$  Gen3 layer (down to  $R_{\text{sheet}} < 20 \Omega/\text{sq}$ ). Using the same laser power on the Gen2 layer results in much higher sheet resistances in the range  $R_{\text{sheet}} = 80-100 \Omega/\text{sq}$ . We therefore conclude that a higher amount of electrically active phosphorous is present in the LBSF created from the Gen3 layer.



**Figure 3:** Measured sheet resistance  $R_{\text{sheet}}$  after laser processing of Gen2 and Gen3  $fPassDop$  layers. Note the semi-logarithmic scale of the graph.

This different amount of active dopant is verified by doping profile measurements acquired by ECV and SIMS as shown in Figure 4. Laser doping from the Gen3 layer yields higher (integrated) dopant content: the surface concentration is in the range of  $N_{\text{surf}} = 3 \times 10^{19} \text{ cm}^{-3}$  compared to the doping from the Gen2 layer being in the range of  $N_{\text{surf}} = 3 \times 10^{18} \text{ cm}^{-3}$  (considering the SIMS profiles). We note that in the case of the Gen2 layer doping, we observe a significant difference between the ECV and SIMS measurement, whereas in the case of Gen3 a far better agreement can be seen. We attribute this to the reduced nitrogen content in the Gen3 layer system in comparison to Gen2.



**Figure 4:** Measured concentration profiles after laser doping from Gen2 and Gen3 layer at a fixed laser power of  $P = 10.1$  W by ECV and SIMS. A higher surface dopant concentration is observed when laser doping from the Gen3 layer.

### 2.3 Nitrogen in laser doped areas

In order to investigate the possible incorporation of nitrogen due to laser doping from the  $fPassDop$  layer system, we measured the atom concentration of phosphorous and nitrogen by SIMS as well. The results for laser doping from Gen2 and Gen3 layers are shown in Figure 5. We observe that a large amount of nitrogen is driven into the silicon during the laser process as well. The concentration is almost two orders of magnitude higher than the one of phosphorous. In the case of Gen3, we see a similar concentration of nitrogen as phosphorous. The electrical effect of this (unwanted) nitrogen is yet to be investigated. However, when comparing SIMS and ECV measurements (shown in Figure 4), a larger amount of nitrogen (as in the case of Gen2) seems to have a larger influence on the ECV measurement. These effects are further discussed in detail by Steinhauser *et al.*[12].

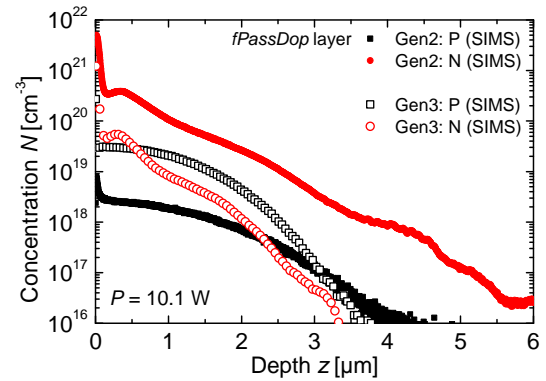


**Figure 5:** Measured atom content of phosphorous and nitrogen after laser doping from Gen2 (closed symbols) and Gen3 layer (open symbols) (acquired by SIMS). Compared to the desired dopant phosphorous, two orders of magnitude higher level of nitrogen is detected in the case of Gen2. Gen3 shows a significant reduction in incorporated nitrogen.

To show whether nitrogen can be detected in the laser doped point contacts, we conducted SEM and along EDX analysis from point contacts generated from both Gen2 and Gen3 layers. This is shown in Figure 6. Whereas in the passivation layer a large amount of nitrogen due to

the  $\text{SiN}_x$  (designated with “1”) and small peaks for phosphorous and oxygen were found, the result in the center of a point contact was different: after laser doping from Gen2 layer (“2a”) peaks for nitrogen and oxygen were detected and after processing of Gen3 layer (“2b”) the nitrogen peak is not detectable anymore. We therefore assume that the amount of incorporated nitrogen is reduced when laser processing using the Gen3 layer. For both layers the phosphorous signal could not be observed as it was below the detection limit of the measurement. Note that integration time during EDX data acquisition is identical for all three data sets as well as the acceleration voltage of the electron beam.

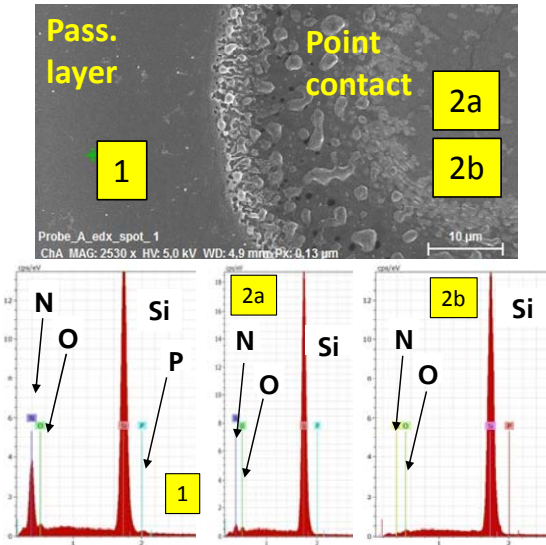


**Figure 6:** Measured energy dispersive x-ray spectroscopy (EDX) from non-lasered and lasered area at a *fPassDop* point contact. 1: EDX spectrum of *fPassDop* passivation layer; 2a: EDX spectrum after laser doping from Gen2 layer, 2b: EDX spectrum after laser doping from Gen3 layer. Integration time during data acquisition is identical for all three data sets.

### 3 SOLAR CELLS

#### 3.1 Solar cell design and process flow

In order to demonstrate the benefit of the modified layer Gen3 compared to Gen2, we fabricated *fPassDop* *n*-type PERL solar cells on both five inch float zone (FZ-Si,  $\rho = 1.0 \Omega\text{cm}$ ,  $A = 149 \text{ cm}^2$ ) and six inch Czochralski (Cz-Si,  $\rho = 1.9 \Omega\text{cm}$ ,  $A = 239 \text{ cm}^2$ ) grown monocrystalline silicon. The fabrication process flow is shown in Figure 7. The rear side was planarized by a KOH etch and the front side was textured with random pyramids using masking layers; the  $\text{p}^+$  emitter was fabricated by thermal  $\text{BBr}_3$  diffusion in a tube furnace. After removal of the borosilicate glass (BSG), the wafers were cleaned and the rear side was passivated by the *fPassDop* layer. Then, a thin layer of  $\text{AlO}_x$  was deposited on the front side for emitter passivation; a  $\text{SiN}_x$  anti reflection coating (ARC) was applied on top. AgAl electrodes were printed on to the front side, where as the busbars consist of a non-firing through Ag paste. After fast firing, the wafers received rear side laser processing (point contact opening and doping) and aluminum was evaporated on top to finish the *n*-electrode. Before *I-V* testing, the cells were submitted to a short forming gas anneal at  $350^\circ\text{C}$ .

FZ-Si, planar	Cz-Si, as-cut
KOH damage etch	
RS masking (therm. $\text{SiO}_2$ )	RS masking (PVD $\text{SiO}_x/\text{SiN}_x$ )
Alkaline texture	
RS mask removal	
$\text{BBr}_3$ emitter diffusion	
BSG etching (incl. RS barrier removal)	Wet chem. rear side emitter removal (incl. BSG etch)
RS <i>fPassDop</i> deposition (PECVD)	
FS $\text{AlO}_x$ (ALD) deposition	FS $\text{AlO}_x$ (PECVD) deposition
FS $\text{SiN}_x$ anti-refl. Coating (PECVD)	
FS dual screen print: AgAl for fingers, Ag for BBs	
Fast firing	
RS PassDop laser processing (opening + doping)	
RS Al evaporation + short FGA	
<i>I-V</i> testing	

**Figure 7:** Process flow for the fabrication of *n*-PERL cells with *fPassDop* rear side scheme.

#### 3.2 Results and discussion

The results, i.e. measured *I-V* data, are shown in Table I. On both base materials, the same trend can be observed: the cells featuring the *fPassDop* Gen2 layer show a lower fill factor as well as a larger scattering thereof compared to the cells passivated with the Gen3 layer. This lower fill factor is attributed to a higher series resistance  $R_s$  (evident in the larger fill factor difference  $pFF-FF$ ) originating from the rear side as for all the cells the front side metallization and fast firing condition were identical for each group of base material. We conclude that the rear side metal-semiconductor contact quality is therefore superior when employing the *fPassDop* Gen3 layer and we attribute this to the higher level of doping in the LBSF as previously shown in Figure 4.

**Table I:** *I-V* results of the fabricated *fPassDop* *n*-PERL cells on both FZ-Si ( $\rho = 1.0 \Omega\text{cm}$ ,  $A = 149 \text{ cm}^2$ ) and Cz-Si ( $\rho = 1.9 \Omega\text{cm}$ ,  $A = 239 \text{ cm}^2$ ). The mean value and the standard deviation are given. The best cell is given for both FZ- and Cz-Si with *fPassDop* Gen3 rear side passivation. Data marked with \* are certified measurements by Fraunhofer ISE CalLab.

Base	<i>fPassDop</i>		$V_{oc}$ [mV]	$J_{sc}$ [mA/cm <sup>2</sup> ]
FZ-Si	Gen2	Mean (4 cells)	$671 \pm 1$	$39.6 \pm 0.1$
	Gen3	Mean (17 cells)	$673 \pm 1$	$39.2 \pm 0.2$
	Gen3	Best cell*	672	39.7
Cz-Si	Gen2	Mean (3 cells)	$663 \pm 2$	$38.6 \pm 0.1$
	Gen3	Mean (4 cells)	$664 \pm 1$	$39.1 \pm 0.0$
	Gen3	Best cell*	665	39.5

Base	<i>fPassDop</i>		$FF$ [%]	$pFF$ [%]	$\eta$ [%]
FZ-Si	Gen2	Mean (4 cells)	$74.0 \pm 2.8$	$83.1 \pm 0.1$	$19.7 \pm 0.7$
	Gen3	Mean (17 cells)	$79.1 \pm 0.7$	$83.2 \pm 0.1$	$20.9 \pm 0.2$
	Gen3	Best cell*	78.6	83.4	20.9
Cz-Si	Gen2	Mean (3 cells)	$74.4 \pm 0.5$	$81.1 \pm 0.1$	$19.0 \pm 0.1$
	Gen3	Mean (4 cells)	$77.7 \pm 0.2$	$82.0 \pm 0.2$	$20.2 \pm 0.1$
	Gen3	Best cell*	77.2	82.3	20.3

We also note that the cells fabricated on FZ-Si base material show an open circuit voltage  $V_{OC} > 670$  mV. Despite the use of screen printed AgAl front contact fingers limiting the cell performance to some extent - as reported by other researchers [13] -  $V_{OC}$ 's within this range or above are possible when using a suitable cell architecture and a dual printing approach. The cells on FZ-Si achieve close to 21% conversion efficiency. The cells on Cz-Si, however, show efficiencies up to 20.3%. This is mainly due to differences in the fill factor and the open circuit voltage, as shown in Table II.

**Table II:** Dissemination of  $I$ - $V$  parameters for the best cells on FZ- and Cz-Si (calibrated measurements)

$I$ - $V$ parameter	Difference: FZ-Si vs. Cz-Si	reason
$FF$ [%]	1.4 %	$pFF$ and $R_s$ ( $pFF$ - $FF$ )
$pFF$ [%]	1.1 %	Material quality and non-perfect rear side masking for Cz-Si
$pFF$ - $FF$ [%]	0.3%	Different front contact layout due different wafer size
$V_{OC}$ [mV]	7	Differences in implied voltage ( $iV_{OC}$ ) of device

The implied voltages  $iV_{OC}$  of the devices (before metallization) was determined by quasi-steady-state photoconductance (QSSPC) and was found to be  $iV_{OC} = 681$  mV for the Cz-Si structure and  $iV_{OC} = 694$  mV for the FZ-Si samples. This difference is due to slightly different processes for the 5- and 6-inch wafers and the base material itself: different recipes in the  $BBr_3$  emitter diffusion and emitter passivation (ALD for FZ-Si, PECVD for Cz-Si), are yielding emitter saturation current densities of  $J_{0e} = 50$  fA/cm<sup>2</sup> for the FZ and  $J_{0e} = 80$ -90 fA/cm<sup>2</sup> for the Cz-Si wafers. This accounts for about 9 mV difference in the  $iV_{OC}$ . The different level of  $pFF$  accounts for about 2 mV, which is attributed to material quality after the high temperature boron diffusion. The different base doping is responsible for about 2 mV different in quasi Fermi-level splitting. However, after cell metallization, only a difference of 7 mV in terminal voltage  $V_{OC}$  remains.

As both the base doping and the emitter formation/passivation can be adjusted/optimized, we believe that values for  $iV_{OC} > 690$  mV are also feasible for Cz-Si and thus  $V_{OC}$  levels above 670 mV are possible for Cz-Si.

#### 4 CONCLUSION

We have shown that the modification of the firing stable *PassDop* layers can yield a higher surface doping concentration after laser processing. We also find that the amount of nitrogen incorporated in the point contact after laser processing is reduced when employing the Gen3 layer stack featuring less nitrogen in the layers themselves. This higher surface concentration of phosphorous is thought to be beneficial for contact formation of the rear side electrodes.

Fabricated solar cells support these findings, as cells featuring Gen3 layers exhibit lower resistive losses and less scattering in  $FF$  compared to cells passivated with the Gen2 layer. The cells achieve 20.9% efficiency and feature open circuit voltages of 672 mV even though screen printed AgAl front side electrodes are used.

#### 5 ACKNOWLEDGEMENTS

We thank Benjamin Lee and Bob Reedy for the support with the SIMS measurements.

#### REFERENCES

- [1] D. Macdonald and L. J. Geerligs, "Recombination activity of interstitial iron and other transition metal point defects in p- and n-type crystalline silicon," *Applied Physics Letters*, vol. 85, pp. 4061-3, 2004.
- [2] J. Schmidt, *et al.*, "Investigation of carrier lifetime instabilities in Cz-grown silicon," in *Proceedings of the 26th IEEE Photovoltaic Specialists Conference*, Anaheim, California, USA, 1997, pp. 13-18.
- [3] S. W. Glunz, *et al.*, "Minority carrier lifetime degradation in boron-doped Czochralski silicon," *Journal of Applied Physics*, vol. 90, pp. 2397-404, 2001.
- [4] R. M. Swanson, "Approaching the 29% limit efficiency of silicon solar cells," in *Proceedings of the 31st IEEE Photovoltaic Specialists Conference*, Orlando, USA, 2005, pp. 889-94.
- [5] S. W. Glunz, *et al.*, "n-type silicon - enabling efficiencies > 20% in industrial production," in *Proceedings of the 35th IEEE Photovoltaic Specialists Conference*, Honolulu, Hawaii, USA, 2010.
- [6] J. Benick, *et al.*, "High-efficiency n-type silicon solar cells with front side boron emitter," in *Proceedings of the 24th European Photovoltaic Solar Energy Conference*, Hamburg, Germany, 2009, pp. 863-70.
- [7] J. Zhao, *et al.*, "24.5% Efficiency silicon PERT cells on MCZ substrates and 24.7% efficiency PERL cells on FZ substrates," *Progress in Photovoltaics: Research and Applications*, vol. 7, pp. 471-4, 1999.
- [8] A. Edler, "Development of bifacial n-type solar cells for industrial application," Mathematisch-Naturwissenschaftliche Sektion - Fachbereich Physik, Universität Konstanz, 2014.
- [9] D. Suwito, *et al.*, "Industrially feasible rear passivation and contacting scheme for high-efficiency n-type solar cells yielding a  $V_{oc}$  of 700 mV," *IEEE Transactions on Electron Devices*, vol. 57, pp. 2032-6, 2010.
- [10] U. Jäger, *et al.*, "A laser based process for the formation of a local back surface field for n-type silicon solar cells," *Thin Solid Films*, vol. 519, pp. 3827-30, 2011.
- [11] B. Steinhauser, *et al.*, "Firing-stable PassDop passivation for screen printed n-type PERL solar cells based on a-SiN<sub>x</sub>:P," *Solar Energy Materials and Solar Cells*, vol. 126, pp. 96-100, 2014.
- [12] B. Steinhauser, *et al.*, "The Influence of Nitrogen on Laser Doping from Phosphorous Doped a-SiN<sub>x</sub> Layers," *submitted to Solar Energy Materials & Solar Cells*, 2015.
- [13] E. Lohmüller, *et al.*, "The HIP-MWT+ solar cell concept on n-type silicon and metallization-induced voltage losses," in *Proceedings of the 29th European Photovoltaic Solar Energy Conference and Exhibition*, Amsterdam, The Netherlands, 2014, pp. 635-41.